# Mapping the dynamical organization of the cell nucleus through fluorescence correlation spectroscopy

Martin Stortz [a,b], Juan Angiolini [b,c], Esteban Mocskos [d,e], Alejandro Wolosiuk [f,g], Adali Pecci [a,h], Valeria Levi [c,h,*]

[a] CONICET – Universidad de Buenos Aires, IFIBYNE, Argentina
[b] Universidad de Buenos Aires, Facultad de Ciencias Exactas y Naturales, Argentina
[c] CONICET – Universidad de Buenos Aires, IQUIBICEN, Argentina
[d] Universidad de Buenos Aires, Facultad de Ciencias Exactas y Naturales, Departamento de Computación, Argentina
[e] CONICET – Centro de Simulación Computacional para Aplicaciones Tecnológicas, Buenos Aires, Argentina
[f] Gerencia Química, Centro Atómico Constituyentes, Comisión Nacional de Energía Atómica, CONICET, Argentina
[g] Universidad de Buenos Aires, Facultad de Ciencias Exactas y Naturales, Departamento de Química Inorgánica, Analítica y Química Física, Argentina
[h] Universidad de Buenos Aires, Facultad de Ciencias Exactas y Naturales, Departamento de Química Biológica, Argentina

## ARTICLE INFO

## ABSTRACT

The hierarchical organization of the cell nucleus into specialized open reservoirs and the nucleoplasm overcrowding impose restrictions to the mobility of biomolecules and their interactions with nuclear targets. These properties determine that many nuclear functions such as transcription, replication, splicing or DNA repair are regulated by complex, dynamical processes that do not follow simple rules. Advanced fluorescence microscopy tools and, in particular, fluorescence correlation spectroscopy (FCS) provide complementary and exquisite information on the dynamics of fluorescent labeled molecules moving through the nuclear space and are helping us to comprehend the complexity of the nuclear structure. Here, we describe how FCS methods can be applied to reveal the dynamical organization of the nucleus in live cells. Specifically, we provide instructions for the preparation of cellular samples with fluorescent tagged proteins and detail how FCS can be easily instrumented in commercial confocal microscopes. In addition, we describe general rules to set the parameters for one and two-color experiments and the required controls for these experiments. Finally, we review the statistical analysis of the FCS data and summarize the use of numerical simulations as a complementary approach that helps us to understand the complex matrix of molecular interactions network within the nucleus.

## 1. Introduction

The last decades have seen rapid advances in our understanding of nuclear organization and function. Diverse techniques, from high-throughput chromatin conformation capture techniques [1] to single molecule methods [2], firmly demonstrated that the nucleus of eukaryotic cells is an intricate organelle having a dynamical organization with different layers of complexity each of them relevant to nuclear function.

A clear example of this complex and functional organization is given by chromatin, the major component of the cell nucleus. During interphase, each chromosome occupies non-random positions in the nucleus referred to as chromosome territories [3,4] that present gene-rich regions mainly oriented towards the nuclear interior and gene-poor regions at the periphery [3–5] This topography is also determined by the interactions of chromatin with nuclear substructures such as the nuclear lamina [6]. Moreover, the chromatin landscape is not static but presents continuous changes at the different organization levels impacting on gene expression and genome maintenance. These changes range from subtle, local modifications on chromatin compaction triggered by architectural chromatin proteins, histone chaperones and

chromatin remodelers (reviewed in [7]) to repositioning of whole chromatin loops [8].

The overcrowding of biomolecules in the nuclear space and the presence of entangled biopolymers means that the intranuclear milieu behaves as a complex fluid [9] presenting a multi-scale porosity that constrains the diffusion of molecules in a size-dependent manner [10]. Thus, molecular diffusion in the nucleoplasm does not follow the simple rules expected for an aqueous environment [10–13].

In addition, many processes are compartmentalized into defined spatial regions named nuclear bodies which are not enclosed by membranes as cytoplasmic organelles [14] and dynamically exchange components with the nucleoplasm [15]. Since these compartments concentrate biomolecules involved in closely related processes, it is proposed that they may increase the efficiency of certain reactions and facilitate their regulation [16]. This aspect of nuclear organization opens relevant questions regarding the mechanisms of bodies assembly, maintenance and exchange of molecules with the nucleoplasm [17].

In this work, we describe how FCS methods can be applied to reveal the dynamical organization of the nucleus. The combination of these approaches with the standard confocal, live cell imaging also provides information regarding the subcellular context at the region selected for FCS measurements. Labeling nuclear structures with specific and different-color fluorescent probes also reveals new aspects on the dynamical distribution of the studied molecule. Although we focus on studies of cultured cells, the methodology may be extended to certain live organisms (for example, [18,19]). We describe how these methods are easily instrumented in commercial confocal microscopes, review the data analysis and summarize the use of numerical simulations as a complementary approach that also help us to understand the interactions network of a molecule within the nucleus.

In particular, we use the glucocorticoid receptor (GR), a ligand-dependent transcription factor, as a representative example of the experimental data attainable with this approach. GR primarily localizes in the cytoplasm, translocates to the nucleus upon ligand binding and interacts directly or through other proteins with DNA targets. Similarly to many components of the transcription machinery ranging from transcription factors (TFs), coregulators, chromatin remodelers and RNA polymerases, the activated GR accumulates in clusters or foci that dynamically exchange molecules with the nucleoplasm [20–23].

## 2. Brief overview of fluorescence microscopy methods for studying the dynamical organization of the cell nucleus

Live cell fluorescence microscopy provides unique tools to visualize the nuclear organization *in situ* and in real time. Particularly, methods such as fluorescence recovery after photobleaching (FRAP) and related techniques [24,25], fluorescence correlation spectroscopy (FCS, [26–28]) and single molecule/particle tracking (SMT, SPT, [29–31]) afford complementary information that helps us to build a more complete view of the different layers of nuclear organization.

Table 1 briefly describes the basics of these methods, focusing in the advantages and disadvantages for studying the dynamics within the cell nucleus; we refer interested readers on this topic to recent reviews that also include, more sophisticated methodologies derived from these basic tools [2,32–34]. We should also mention that relatively new, spatio-temporal correlation approaches based on scanning the laser on the sample and correlating the intensity collected at different positions provides exquisite information on molecules dynamics. For example, a crosscorrelation analysis of the intensity traces recorded at two different positions allows extracting information of molecules that move from one position to the other and permits quantifying diffusion, flow or even detecting obstacles or barriers to the motion [12,35–38].

### 2.1. Preparation of fluorescently-tagged cells for FCS measurements

The first step in every FCS measurement in living cells comprises the selection of protocols for tagging the biomolecule of interest with a fluorescent probe and delivering it into the cellular system. FCS measurements require fluorophore concentrations in the nanomolar range [39]; lower or higher amounts of fluorescent molecules may result in either poor statistics or a low amplitude of the autocorrelation functions. This can be sometimes solved increasing the acquisition time [40].
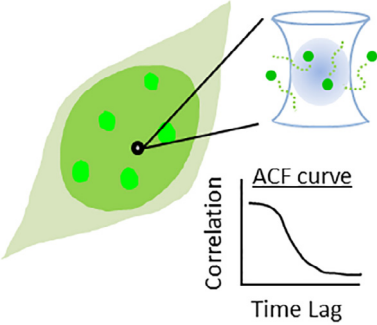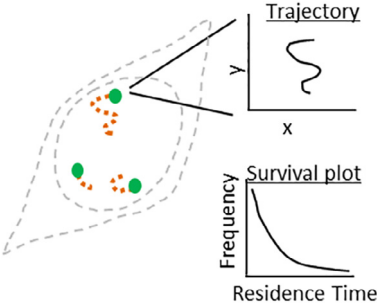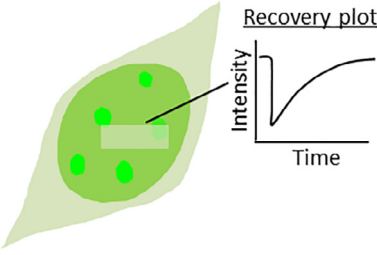
The modification of proteins with fluorescent probes is achieved by different strategies including the purification of the protein, its labeling with a synthetic dye and the cell delivery with the aid of microinjection [41], the expression of the protein linked to tags that react with modified versions of the probe [42] and more frequently, the expression of the biomolecule fused to variants of fluorescent proteins. We will focus in this last approach since this is a widely used method to label proteins for FCS experiments. The applications of fluorescent proteins have expanded enormously from the initial discovery and characterization of the green fluorescent protein (GFP, reviewed in [43]) and they are now routinely used for the observation of biomolecules in living specimens. We refer the readers to excellent reviews in the field [44,45] and only provide a few guidelines for their uses in FCS measurements.

Although many researchers use pre-existing plasmids in their labs, it is important to check whether the properties of the fluorescent protein encoded in the plasmid are adequate for FCS measurements. A large compendium of both photophysical and biochemical properties of fluorescent proteins can be found in the literature [46]. In this context, two photochemical/photophysical parameters of fluorescent probes are of paramount importance for FCS measurements: brightness and photostability. The former accounts for the number of photons emitted per second by the fluorescent probe, being related to the product between the fluorescence quantum yield of the probe and its absorption coefficient [47]. Evidently, increasing the brightness of the dye improves the signal to noise ratio of FCS measurements [48]. On the other hand, the dye photostability must be considered as photobleaching processes represent a serious problem in FCS experiments as will be discussed below.

The expression of the fluorescent, fusion protein can be achieved either by transient transfection protocols or by preparation of stable cell lines. Transient transfection involves the introduction of plasmidic DNA to the cells with the aid of a transfection reagent; the expression of the exogenous gene normally persists for 24–72 h after this procedure. Although this technique is methodologically simple and fast, the expression levels within the cell population are not homogeneous and follow a wide normal distribution. Fortunately, the expression level may be quantitatively manipulated by changing the plasmidic DNA/cells ratio [49]. This fact opens the possibility of performing fluorescence fluctuations experiments within a broad range of protein concentrations and to modulate concentration ratios in two-color experiments.

Conversely, the stable transfection procedure involves the integration of the gene of interest into the chromosomal DNA and thus the creation of a cell line, the wisest choice for long-term experiments. This procedure invariably uses a strategy to select the transfected cells which involves the addition of a gene that confers resistance (positive selection) or sensitivity (negative selection) to an added drug. Stable transfection provides a more homogeneous and relatively low concentration of the fluorescent protein in every

**Table 1**
Principles of fluorescence microscopy methods commonly used to study nuclear dynamics.

| Method | Scheme | Principles | Advantages | Disadvantages | Examples |
|---|---|---|---|---|---|
| FCS |  | Fluorescent molecules moving through the observation volume introduce fluctuations in the intensity time trace. The fluctuations are quantitatively analyzed to extract through correlation analyses information on the molecules dynamics. | • Minimal photodamage.<br>• Requires low concentration of fluorescent molecules.<br>• High temporal and spatial resolution. | • Poor detection of very slow and/or infrequent events. | [18,23,27,28] |
| SMT/SPT |  | Individual molecules/particles are imaged as a function of time; their trajectories are recovered using tracking routines with subpixel resolution. The analysis of the trajectories inform on the mechanism of motion. Immobile molecules are identified as bound molecules and the duration of these events provide the residence time at the sites. | • Requires low concentration of fluorescent molecules.<br>• Detect slow and infrequent events.<br>• Map a large area in each measurement. | • Generally requires more sophisticated equipments.<br>• Low temporal resolution. | [31,111–115] |
| FRAP |  | A specific region of the nucleus is photobleached using a high laser power. The recovery of fluorescence intensity in the photobleached region is monitored as a function of time and analyzed to obtain information on the molecules mobility. | • Easy and straightforward instrumentation.<br>• Simple data analysis. | • Photodamage<br>• Requires a relatively high concentration of fluorescent molecules.<br>• Low spatial resolution.<br>• Low temporal resolution. | [116,117] |

cell, which may be desirable for FCS measurements. However, the procedure is usually laborious and time consuming (~1–3 months) delaying the natural course of scientific research. In addition, stably transfected cell line may adapt to the expression of the introduced gene resulting in different physiological behaviors of the fluorescent cell line and the parental cells [50].

The use of expression vectors codifying the fluorescent protein under the control of weak promoters allows obtaining low protein concentration appropriated for FCS studies independently of the transfection procedure. Another option is the use of conditional-promoters sensitive to an administered drug, which will control the protein expression level. Many versions of these inducible promoters are available from commercial sources.

More recently, the development of type II CRISPR/Cas technology marked the beginning of a new era in genetic engineering and, particularly, in fluorescent protein labeling [51]. The system consists in a RNA-guided dsDNA endonuclease and allows performing knock-in experiments by homologous or non-homologous recombination [52]. The RNA guide sequence provides the possibility to specifically target a *locus* in the genome and to obtain a fluorescently labeled protein in its own genomic context, with an endogenous gene expression [53]. Also, the Cas endonuclease can

be fluorescently labeled, giving the chance to label specific DNA sequences and thus to study its dynamics by imaging [54].

Cells should be monitored after any of these transfection procedures to verify that the fluorescent molecules are not affecting their health. As a first approach, it is important to compare the subcellular distribution of the fluorescent and endogenous proteins and their response to specific and known stimuli [55]. In some cases, the fluorescent tag may introduce a structural modification of the biomolecule that could lead to an aberrant subcellular localization, its aggregation and/or a change in its function [55]. In the case of proteins involved in the regulation of transcription, it is advisable testing the transcriptional activity of the fluorescence labeled constructs through gene-reporter assays [56,57]. In addition, many fluorescent proteins self-associate introducing artifacts in either the localization (reviewed in [58]) or the mobility of the tagged-protein. These effects may also be caused by anomalous high concentrations of the fluorescent molecules [59].

The single-cell concentration of the expressed protein could be estimated by different fluorescent approaches (e.g. [60–63]). The easiest procedure consists on correlating intensity levels to protein concentrations using a standard of known concentration of the fluorescent protein. We should advice that this method stands on two

assumptions: 1) identical brightness of the fluorescent protein in the standards and the sample [64] and 2) homogeneous distribution of the proteins in the region of interest. Again, this last statement is usually invalid in the heterogeneous nucleus as we described before.

Cells are normally plated on #1.5 glass coverslips (0.17 mm thickness, adequate for high-numerical aperture objectives). Coverslips may often need to be pre-coated with an extracellular matrix component, such as fibronectin, collagen, polylisine or laminin to improve the cells adhesion to the glass and minimize their motion during the acquisition of fluorescence fluctuations data; different protocols for cleaning and coating the coverslips have been described elsewhere (e.g. [65]).

### 2.2. Setting up a commercial microscope for FCS and FCCS measurements in the nucleus

#### 2.2.1. General overview

Different FCS-based strategies can be combined to get insights into the intranuclear dynamics. These methods rely on the quantitative analysis of temporal and/or spatial traces of the fluorescence intensity acquired in fluorescence microscopes with z-sectioning capability such as confocal or multiphoton-excitation [66–68], total internal reflection and light sheet [69–71] and even more sophisticate, superresolution microscopes [72,73]. Particularly, confocal microscopy achieves a femtoliter-sized observation volume with ellipsoidal 3D-Gaussian shape [68] at relatively low laser powers [74].

In the simplest confocal FCS experiment, the laser is placed at a fixed position of the specimen using preferably either water or silicon oil immersion objectives with high numerical aperture and the fluorescence intensity is collected at the optically-defined observation volume as a function of time. Despite it is a worldwide common practice to use oil immersion objectives for observing or running FCS experiments in cultured cells due to the lower cost of these objectives, the mismatch between the glass/oil and water medium introduces aberrations and reduces the resolution of the setup; these effects get worst as the objective focuses deeper in the sample [75]. We normally run the FCS experiments at the z-center of the nucleus i.e. at similar z-positions with respect to the coverslip since the cell thickness does not vary too much between cells (not shown).

Fig. 1 shows typical ACF data obtained for dexamethasone-activated GR in the nucleus of BHK cells, also illustrating the heterogeneous, dynamical distribution of the receptor. When the purpose of the experiment is to study the dynamics of a biomolecule at certain regions of the nucleus, it is desirable to label these regions with a specific, different-color probe for their easy and simultaneous identification.

When possible, it is not recommendable to run many point-FCS experiments in a single nucleus as photodamage alters significantly the nuclear dynamics [76]. Alternatively, the dynamics can be assessed using point-FCS measurements in several cells; each data is analyzed independently obtaining distributions of parameters characterizing the dynamics. The number of cells required for this analysis depends on: i) inter- and intra-nuclear heterogeneities in the fluorescent molecules dynamics; ii) the expected distribution for the parameters and iii) the intrinsic noise in the measurements. As a rule of thumb, we normally start our studies with at least 30 cells to reach a conclusion with statistical significance.

#### 2.2.2. Calibrating the commercial microscope for FCS measurements

The first step in every FCS experiment is characterizing the observation volume in identical instrumental conditions to those used for the FCS measurements in the cells. Specifically, the measurements should be run with the same objective, the same laser wavelength and laser power since the observation volume depends critically on these parameters [77]. The derivation of different expressions for the FCS correlation function normally assumes that the fluorescence intensity is proportional to the intensity of the excitation light; this assumption is only valid at low laser intensities [40].

The pinhole should be correctly aligned to optimize FCS measurements. Most modern, commercial microscopes do not require daily adjustments of the pinhole position as many home-built microscopes do. However, the user can check and center laterally the pinhole following the procedures described in the literature for a commercial setup [78].

In most FCS analyses, the shape of the observation volume is assumed to be that predicted from theory (e.g. a 3D Gaussian for a confocal microscope). In this case, the characteristic dimensions of the volume are obtained in calibration experiments using an aqueous solution of a probe of known mobility [79]; the diffusion coefficient (D) of free dye fluorescent probes in aqueous solution lie in the 300–450 $\mu m^2$/s range (data compiled in [80]). In order to generate standards with D values in the range of those observed for biomolecules within the nucleus, we usually add glycerol to
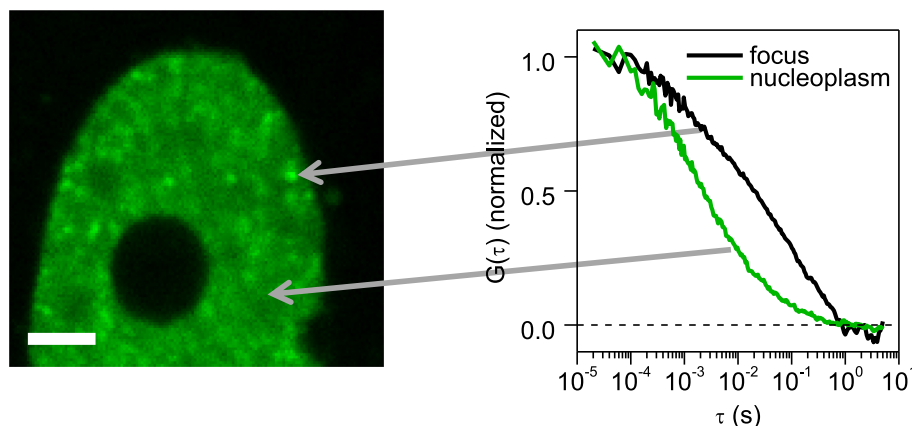


**Fig. 1.** Exploring the dynamics of a transcription factor in the heterogeneous nuclear environment by FCS. BHK cells expressing the glucocorticoid receptor (GR) fused to GFP and stimulated with dexamethasone were imaged by confocal microscopy (left panel, scale bar: 2 μm). GR accumulates in numerous discrete foci within the nucleus. Single-point FCS measurements were performed at the nucleoplasm and a focus, in the same cell. Right panel shows the normalized ACFs and illustrates the dynamics heterogeneity of the receptor.

increase the viscosity of the solution. For instance, adding 25% glycerol reduces 50% of a probe diffusion coefficient compared to pure water. Alternatively, a protein of known hydrodynamic radius can be chemically modified with a fluorescent probe and used as a standard with diffusion coefficient closer to those observed in living cells. Whit this aim, we chemically modify BSA (bovine serum albumin) with FITC [81]. The Stokes radius of this protein is ∼3.48 nm [82] and thus the diffusion coefficient in an aqueous solution is ∼6 $\mu m^2$/s as estimated from the Stokes-Einstein equation [83]. We normally add to the medium a relatively low concentration of a chaotropic agent (0.5 M guanidinium chloride) to minimize the aggregation of the protein. Previous studies showed that the protein preserves its folded conformation at this relatively low concentration of denaturant [84].

Finally, the detectors afterpulse should be characterized before performing FCS experiments [48]. These experiments involve counting photons using either APDs (avalanche photodiodes) or PMTs (photomultiplier tubes). Both detectors present afterpulse noise that consist on registering spurious signals, shortly after an event of photon detection [85]. As a consequence, afterpulses introduce a positive correlation at short lag times as observed in Fig. 2A. The temporal window of the afterpulse can be characterized registering an intensity trace with the microscope shutter closed; in this simple experiment only dark counts are registered and the correlation curve results from the afterpulse noise. Typically, the correlation due to afterpulse is in the microsecond window, much faster than the dynamics of molecules in the nucleus and thus it does not interfere with the FCS measurements (Fig. 2A). To analyze the experimental data, we set a lag time threshold (in the case of the data showed in Fig. 2A, the threshold was 20 µs) avoiding the observation of the afterpulsing signal and capturing the dynamics of the molecules. When afterpulsing
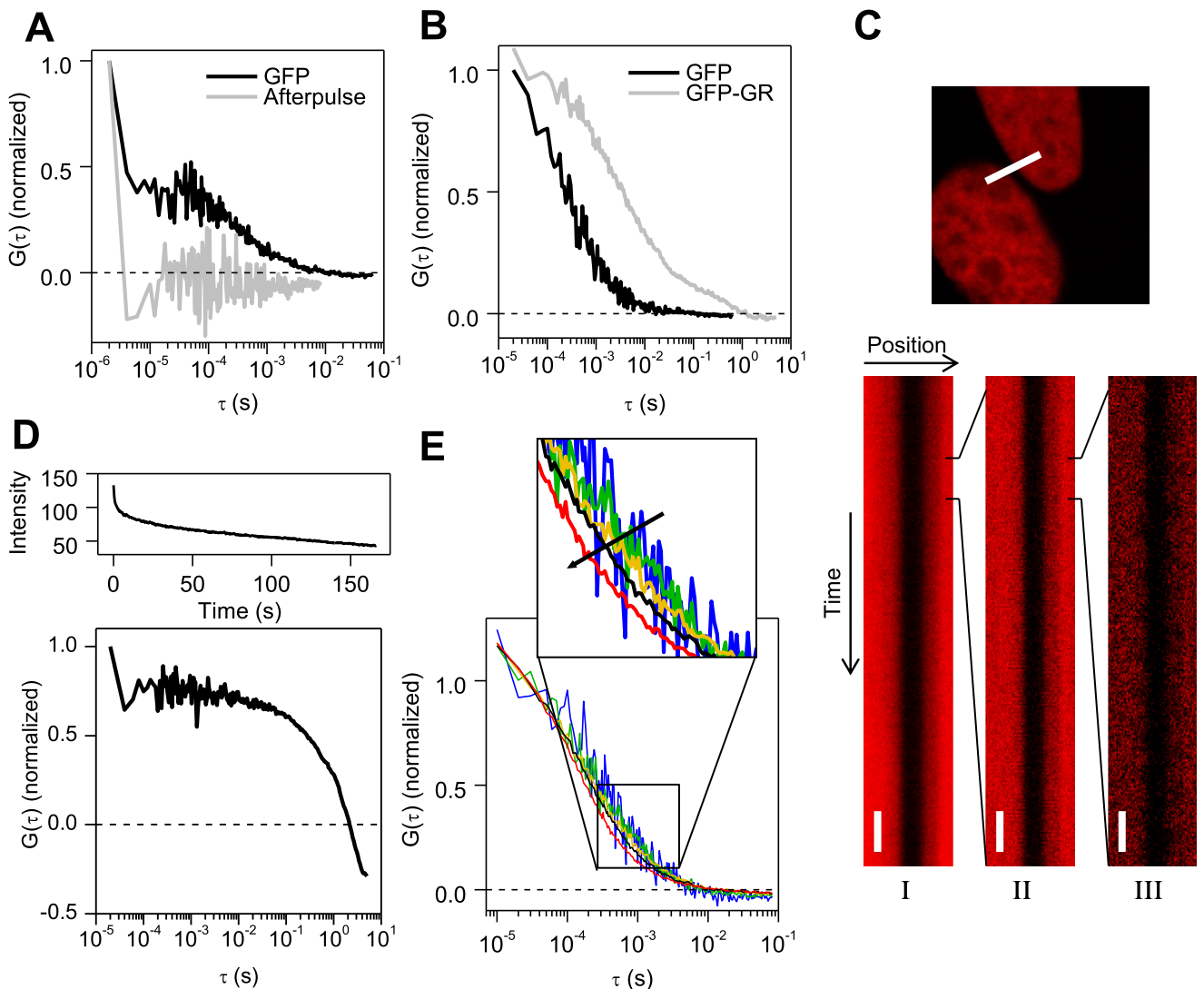


**Fig. 2.** Setting up the acquisition parameters for FCS measurements. Special care must be taken during FCS analysis to detect problems derived from inadequate acquisition of FCS data. (A) The afterpulse noise introduces a high correlation at short lag times. In the Olympus FV1000 detectors, the afterpulse occurs in a time window <4 µs, and does not hamper the measurements of dynamics within the nucleus, even for a fast moving protein as GFP. (B) GFP-GR fusion protein presents a delayed dynamics respect to GFP in the nucleus of BHK cells, due to the interaction with chromatin and other proteins. (C) Assessing the motion of the nucleus in the time window of FCS experiments. BHK cells transiently expressing H2B-mCherry were imaged by confocal microscopy. The laser was repetitively scanned during 24 s along a 5 µm-line (white line) that intersects two nuclei setting the pixel size to 80 µm. The fluorescence intensity collected along the line as a function of time is shown at three different time scales. White bars represent 1 s (I), 100 ms (II) and 10 ms (III). (D) Drastic photobleaching processes can be easily detected in both, the intensity time trace and the ACF. In this example, the photobleaching is highly significant and the ACF curve does not relax to zero thus, the data should be discarded from the analysis. (E) FCS measurements were performed in the nucleus of a BHK cell expressing GFP-GR at different laser powers (blue: 2.1 µW; green: 2.4 µW; yellow: 4.1 µW; black: 11 µW; red: 24 µW; the arrow points in the direction of increasing laser powers). (For interpretation of the references to color in this figure legend, the reader is referred to the web version of this article.)

temporally overlaps with the dynamics of the molecules, its contribution to the ACF curve could be removed by relatively simple experimental or theoretical methods (e.g. [86]).

### 2.2.3. Setting up the parameters for the acquisition of single-point FCS data in the cell nucleus

*2.2.3.1. Selecting the acquisition frequency and total acquisition time.* We have mentioned previously that the nucleus is an overcrowded and highly viscous environment introducing a significant drag to the diffusion of molecules. Molecular interactions with nuclear targets such as chromatin may also delay the molecule motion as exemplified in Fig. 2B. The figure shows representative ACF curves obtained for GFP fusion proteins in the nucleus of BHK cells; GR-GFP presents a delayed dynamics respect to GFP as a consequence of interactions with chromatin and other proteins. The protein mobility should be taken into account when setting both, the acquisition frequency and the total acquisition time of FCS experiments. These parameters depend on the characteristic time of the intensity fluctuations ($t_c$). A rule of thumb for estimating $t_c$ is to use the Stokes-Einstein equation [83] considering the size of the biomolecule and a nuclear viscosity $\sim$5 times higher than water [11]. Despite the real mobility could be far from this estimation, it is a good starting point.

The sampling time should be $\sim$2/3$t_c$ to optimize the observation of the ACF curve with optimal S/N ratios [87] and the total duration of the experiment should be $10^4\ t_c$ to obtain a $\sim$1% precision on this parameter [68]. In some cases, the duration of the experiment may also be limited by the cell motion; when possible, it is recommendable to modify the glass substrate as described in Section 2.1 to minimize cell movements. In most of our experiments, we acquire data for of 2–3 min using a sampling time of 10–20 μs.

*2.2.3.2. Assessing nuclear motion during FCS measurements.* It is also very important to test whether the nucleus moves during the intensity acquisition since this motion may introduce artifacts in the autocorrelation data. Relatively large movement of the whole nucleus or nuclear substructures can be detected by comparing images acquired before and after the FCS measurements.

Additionally, it is a good idea to characterize the overall movement of the nucleus in the specific cell line within the time window of ACF analyses ($\sim$5 s). Fig. 2C shows an experiment designed to test movements of the nucleus in BHK cells expressing H2B-mCherry; the data did not reveal appreciable translations of the whole nucleus.

Control experiments using cells expressing mutant versions of the biomolecule with impaired biological function could also very useful to rule out artifacts introduced by intracellular motions of nuclear substructures. For example, we run FCS experiments in cells expressing mutant or inactive forms of the TFs with impaired DNA binding capability when studying the dynamics of transcription factors in the nucleus [18,23]. The comparison between data obtained for the wild type and the mutant proteins helped us to recognize TF-DNA interactions in the ACF data and rule out artifacts due to motion of nuclear structures.

*2.2.3.3. Setting the laser power for FCS.* The laser power is also a key parameter to recover the dynamics of molecules. As in every fluorescence microscopy experiment in living cells, the laser power is a compromise between a high S/N and low photobleaching and cell photodamage. In some cases, photobleaching reduces the local concentration of fluorescent molecules, decreasing the mean fluorescence intensity; Fig. 2D shows an FCS experiment in the nucleus of a BHK cell expressing mCherry-GR. The top panel shows that the intensity decreases as a function of time due to photobleaching. Since the intensity does not fluctuate around a mean value, the ACF curve decreases to values below zero at long lag times; in this

case, photobleaching masks the dynamics of the molecules and the ACF analysis does not provide information on this dynamics.

Photobleaching may also affect the correlation data even in cases where there is not an evident reduction in the mean intensity. This may happen when the pool of fluorescent molecules is high and photobleached molecules are replaced by fluorescent molecules. In these cases, the intensity trace may show an initial decay until reaching a constant steady state value. Despite the intensity being constant, molecules turn off before leaving the observation volume and shift the correlation curve to shorter time lags. To set the optimal power laser, it is advisable to acquire FCS data at different powers (Fig. 2D). Very low laser powers introduce noise in the ACF data whereas very high powers cause photobleaching of molecules while they move through the confocal volume shifting the correlation curve to lower τ values. The optimal power corresponds to the value that provides the higher S/N with no shifting in the correlation curve. Usually, the software of commercial confocal microscopes expresses the laser power as a relative value since the absolute power of the laser decays with time. In effect, a "10%" laser power is meaningless; the laser power should be regularly measured at the sample (i.e. placing a power-meter above and close to the objective) to guarantee full reproducibility conditions of the measurements. This procedure only provides a rough estimation of the power at the sample when using a high NA immersion objective since part of the incident light diffracted or reflected at the coverslip that propagates at big angles cannot be collected at the detector. The collection efficiency can be improved using power meters with large-area sensors compatible with dry, water Immersion, and oil immersion objectives. Alternatively, Matsuo et al. [88] proposed placing a solid immersion lens on top of the coverslip to collect with the lens the high-order diffracted light. All these procedures allow testing variations of the laser power in a day-to-day basis that may have an important impact on FCS measurements.

### 2.2.4. Detecting interactions in the cell nucleus with FCCS

*2.2.4.1. General concepts.* Two-color FCCS is an exceptionally useful tool to detect molecular interactions [89]. Molecules A and B are labeled with probes that emit fluorescence in different spectral ranges and intensity traces are simultaneously collected using two channels of the confocal microscope. When these molecules directly or indirectly associate, they move together through the observation volume causing simultaneous fluctuations in the intensity traces collected independently at two channels of the microscope. These fluctuations can be captured through the cross-correlation function ($G_{1,2}(\tau)$):

$$G_{1,2}(\tau) = \frac{\langle \delta I_1(t) \cdot \delta I_2(t+\tau) \rangle}{\langle I_1(t) \rangle \langle I_2(t) \rangle} \tag{1}$$

where $I_{1(2)}(t)$ is the fluorescence intensity as a function of time from channels 1(2) and τ is the lag time.

Fig. 3A shows representative FCCS data obtained in the nucleus of BHK cells expressing GFP-GR and its coactivator mCherry-NCoA-2. The positive cross-correlation function reveals simultaneous fluctuations in the intensity traces in the channels and thus indicates that GFP-GR associates with mCherry-NCoA-2. Fig. 3B shows FCCS data obtained in cells cotransfected with plasmids expressing GFP and mCherry. These molecules move independently from each other determining the absence of cross-correlation.

*2.2.4.2. Calculation of the apparent association constant.* The analysis of $G_{1,2}(\tau)$ provides information about the dynamics of the heterocomplex A-B whereas the amplitudes of the auto and cross-correlation functions are related to the concentrations of the species [90]:
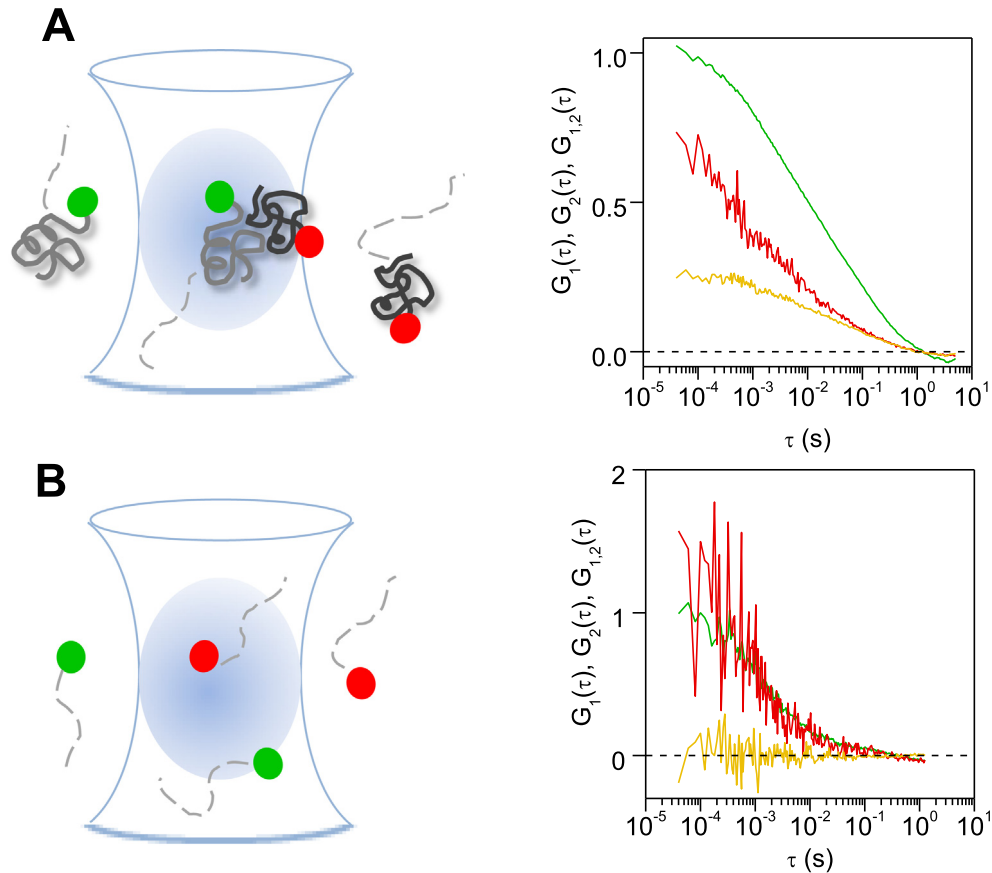
**Fig. 3.** Two-color FCS experiments to analyze interactions in living cells. The interactions between two different proteins in the nucleus can be studied by FCCS, tagging them with different fluorophores (e.g. GFP and mCherry), and detecting simultaneously their fluorescence into two detectors. The intensity traces collected in the detectors are used to calculate the ACFs (green: GFP channel; red: mCherry channel) and the cross-correlation function (yellow). The correlation functions are normalized to the ACF amplitude obtained for GFP. (A) Interactions between GFP-GR and its coactivator mCherry-NCoA-2 in the nucleus of BHK cells stimulated with dexamethasone. (B) Negative control performed in the nucleus of BHK cells expressing GFP and mCherry. (For interpretation of the references to color in this figure legend, the reader is referred to the web version of this article.)

$$[A]_{Free} = \frac{\gamma}{G_1 \cdot N_{av} \cdot V_{PSF}} - [AB]$$

$$[B]_{Free} = \frac{\gamma}{G_2 \cdot N_{av} \cdot V_{PSF}} - [AB] \qquad (2)$$

$$[AB] = \frac{\gamma \cdot G_{1,2}}{N_{av} \cdot V_{PSF} \cdot G_1 \cdot G_2}$$

where $\gamma$ is a geometric factor that depends on detection profile and acquire values of 0.35 and 0.076 for confocal and two-photon excitation profiles, respectively [91]; $\omega_r$ and $\omega_z$ are the radial and axial waist of the observation volume ($V_{PSF} = \omega_r^2 \cdot \omega_z \cdot (\pi/2)^{3/2}$), $N_{av}$ is the Avogadro number and $G_1$, $G_2$ and $G_{1,2}$ are the amplitudes of the auto and cross-correlation functions.

The affinity between the labeled molecules can be estimated calculating the *in situ* apparent association constant ($K_{app}$) as the ratio of the complex concentration to the concentrations of the free species [23,92]. We should emphasize that $K_{app}$ does not take into account the stoichiometry of the interaction and/or the possible binding of monomers and heterocomplexes to other targets that may shift the equilibrium.

*2.2.4.3. Controls and considerations for FCCS experiments.* When selecting the fluorophores, it is usually recommendable avoiding pairs with high FRET probability or significant spectral overlap in their emission. Spectral crosstalk, that may cause false positives, could be minimized combining green and far-red probes [93].

One of the most important considerations in FCCS analysis is using adequate controls for negative and positive cross-correlation. First, the autofluorescence of the cells should be tested in control experiments to verify that it does not introduce artifacts in the standard FCCS measurement conditions. In addition, to check that the spectral crosstalk does not affect the measurements, it is recommendable running control FCCS experiments in cells expressing only one of the labeled proteins or co-expressing only the pair of fluorescent tags; the cross-correlation function should be minimal in this condition (Fig. 3B). Another good practice consists in including a positive control to check the observation volume overlap when using different laser lines. This can be done using a protein fused to both fluorescent probes providing the maximum cross-correlation attainable in the experimental setup.

### 2.3. Data analysis

So far, we have described the procedures required for obtaining traces of fluorescence intensity as a function of time. The experimental data should be carefully analyzed in order to obtain the autocorrelation function (ACF). In our case, we use the SimFCS software (Laboratory for Fluorescence Dynamics, Irvine, CA, USA) or specific MATLAB routines to do this calculation; other alternatives and software packages are available for these analyses (e.g. [94]).

The fundamentals for obtaining the ACF involve dividing the intensity traces into identical-sized segments and calculating the correlation segment-to-segment; finally, the ACF is obtained from an average between the individual ACFs (Fig. 4A). The user should
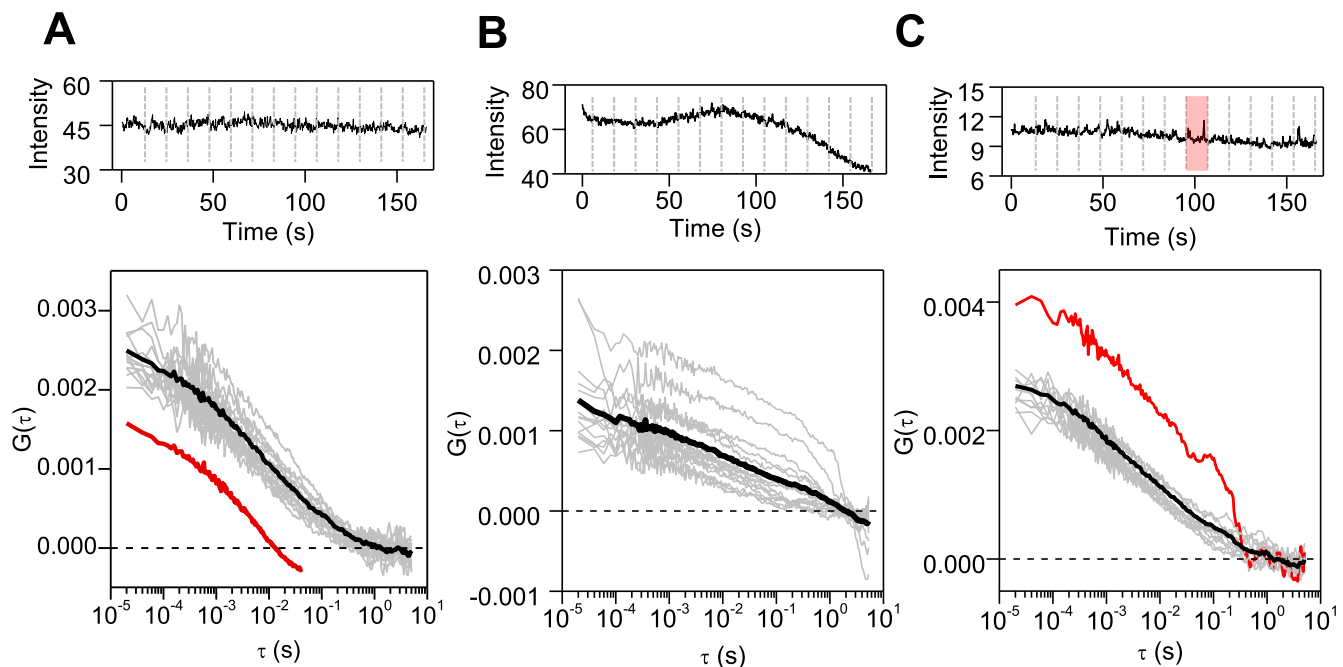
**Fig. 4.** Hints and troubleshooting during FCS analysis. Single-point FCS measurements were performed at the nuclei of BHK cells expressing GFP-GR and stimulated with dexamethasone. The intensity traces (top panels) were divided into identical-sized segments (dotted lines) and the ACF (bottom panels) is calculated segment-to-segment (gray curves) to obtain the average ACF (black curve). (A) The appropriate segment size should be chosen according to the time window of the process(es) causing the fluctuation; the gray and black lines show the segment-to-segment and mean ACF obtained with the correct segment size whereas the red line shows the mean ACF obtained for shorter segments. (B) The slow movement of big structures or large-scale cellular motion introduces slow and large changes in the intensity trace. The ACF does not relax to zero and present high segment-to-segment variability. (C) Anomalous fluctuations due to the movement of an aberrant fluorescent aggregate result in an ACF segment (red curve) that clearly diverges from the rest of the data. In this case, it is safe to remove the outlier curve from the analysis. (For interpretation of the references to color in this figure legend, the reader is referred to the web version of this article.)

set the size of the segment assuming that fluctuations relax within this window; i.e. the ACF approaches zero, and the statistics in every region of the curve is the optimal [48] to obtain accurate parameters from the fitting (Section 2.4). To illustrate this point, Fig. 4A shows the mean ACF recovered when analyzing segments of 5.2 s (black line) or 0.041 s (red line) of the same intensity trace (top panel). Whereas the first case shows the "ideal" behavior (e.g. the ACFs decay to zero and show little segment-to-segment variability), the ACF does not relax to zero in the last case. As we mentioned before, processes in the nucleus are normally slower than in the cytoplasm and thus the temporal window selected for ACF analysis is 2–5 s.

Fig. 4B and C show common problems observed in FCS experiments in living cells. Particularly, Fig. 4B shows slow changes of the intensity as a function of time probably due to the slow movement of structures through the confocal volume. Consequently, there is a high variability among segments and the average ACF curve does not relax to zero in this temporal window. As these processes do not relax within the analyzed temporal window, the ACF function decays below zero and the data is discarded from the analysis. Alternatively, detrend routines (e.g. [95]) could be used to filter out the slow intensity changes when they occur in a very different time scale that the motion of the molecules; for example, these routines are very useful to remove the photobleaching of immobile structures and only analyze the motion of mobile molecules.

The intensity trace observed in Fig. 4C shows a marginal, slower fluctuation that relaxes within the temporal window of the experiment that could be caused by, for example, an aggregate of the fluorescent protein. The individual, ACF curves obtained for the segments that include the slow fluctuation diverges from the mean behavior, then, these outlier segments are normally removed from the analysis.

### 2.4. Extracting quantitative information from ACF curves

The initial step to analyze ACF curve is postulating a theoretical description of the process causing the fluctuations and, in the easiest case, derives a function to fit the experimental data. Such equations have been solved for simple scenarios [96].

Previous works showed that the dynamics of many biomolecules within the cell nucleus does not follow Brownian diffusion and thus the autocorrelation data has been fitted with more complex models summarized in Table 2, some of them include anomalous subdiffusion. This regime refers to diffusional processes with a sub-linear dependence of the mean squared distance with the lag time, consequence of interactions with targets [97] or collisions with obstacles [98].

The initial model is selected based on previous biochemical and biophysical knowledge on the molecules dynamics; it is always necessary validating the model with control experiments. For example, in the case of TFs, the model should include TF-DNA interactions since they are expected to delay TFs motion; using mutants with impaired ability to bind DNA may help to experimentally test the model as we mentioned before.

In some cases, it is useful to statistically compare how different models fit the experimental data. Specifically, the model selected should have the best fit (i.e. no bias and the smallest sum of squared residuals) with the lowest number of parameters. These requirements are included in the Akaike information criterion (AIC, [99]):

$$AIC = 2k - 2\ln(L) \qquad (3)$$

where k is the number of parameters of the model and **L** is the maximum value of the likelihood function for the model; the preferred model is the one that provides the minimum AIC value.

**Table 2**
Interpreting FCS data in the cell nucleus.

| Model | Equation[*] | References |
|---|---|---|
| 2 component's of normal diffusion | $G(\tau) = \frac{1}{2^{3/2}\langle N \rangle}\left[ f_1\left(1+\frac{\tau}{\tau_{D,1}}\right)^{-1}\left(1+\frac{\tau}{\omega^2\tau_{D,1}}\right)^{-1/2} + f_2\left(1+\frac{\tau}{\tau_{D,2}}\right)^{-1}\left(1+\frac{\tau}{\omega^2\tau_{D,2}}\right)^{-1/2}\right]$ | [26] |
| anomalous subdiffusion | $G(\tau) = \frac{1}{2^{3/2}\langle N \rangle}\left(1+\frac{\tau}{\tau_D^\alpha}\right)^{-1}\left(1+\frac{\tau}{\omega^2\tau_D^\alpha}\right)^{-1/2}$ | [11] |
| normal + anomalous subdiffusion | $G(\tau) = \frac{1}{2^{3/2}\langle N \rangle}\left[ f_1\left(1+\frac{\tau}{\tau_{D,1}}\right)^{-1}\left(1+\frac{\tau}{\omega^2\tau_{D,1}}\right)^{-1/2} + f_2\left(1+\frac{\tau}{\tau_{D,2}^\alpha}\right)^{-1}\left(1+\frac{\tau}{\omega^2\tau_{D,2}^\alpha}\right)^{-1/2}\right]$ | [118] |
| fast diffusion + binding | $G(\tau) = \frac{1}{2^{3/2}\langle N \rangle}\left[ f_D\left(1+\frac{\tau}{\tau_D}\right)^{-1}\left(1+\frac{\tau}{\omega^2\tau_D}\right)^{-1/2} + f_b e^{-\tau/\tau_b}\right]$ | [28] |
| fast diffusion + short-lived binding + long-lived binding | $G(\tau) = \frac{1}{2^{3/2}\langle N \rangle}\left[ f_D\left(1+\frac{\tau}{\tau_D}\right)^{-1}\left(1+\frac{\tau}{\omega^2\tau_D}\right)^{-1/2} + f_{fast} e^{-\tau/\tau_{fast}} + f_{slow} e^{-\tau/\tau_{slow}}\right]$ | [18,23] |

[*] $\langle N \rangle$ is the mean number of fluorescent molecules in the confocal volume, $\tau_D$ is the characteristic diffusion time, $\omega$ is the ratio between axial and radial waists of the observation volume, $f_i$ is the fraction of fluorescent molecules moving according to process i, $\alpha$ is the anomaly parameter ($\alpha < 1$ for subdiffusion) and subscripts d, b, fast and slow stand for diffusion, binding, fast binding and slow binding, respectively.

### 2.5. Modeling complex processes: The FERNET fluorescence emission recipes and numerical routines toolkit platform

The modeling of ACF data with analytical solutions is restricted to a very small number of simple scenarios; dynamical processes in the cell nucleus often present a level of complexity that cannot be interpreted only by these simple models.

Recently, we have developed FERNET [100] to understand and interpret ACF data from FCS experiments in complex biological scenarios. FERNET is a software toolkit that includes a Monte Carlo simulation engine (provided by MCell simulation tool, [101–103]), the CellBlender plugin for Blender for geometry design (Blender, http://www.blender.org) and a set of fluorescence simulation routines. This package allows the simulation of a wide variety of FCS experiments from single and multiple point FCS, photon counting histogram analysis, raster image correlation spectroscopy and two-color fluorescence cross-correlation spectroscopy.

In essence, we define the geometry of the scenario (that may include, for example, different compartments) using the MCell program combined with the Blender-CellBlender plugin. Later, we add molecules and set a combination of equations that represent the kinetic-diffusion reactions and processes under study; these equations may include binding and chemical reactions. In addition, the molecular brightness of the species is defined in order to perform fluorescence simulations with FERNET.

FERNET allows simulating fluctuation-based experiments in realistic 3D scenarios where molecules diffuse through different compartments in 2D or 3D fashion, bind to targets or to other species, suffer reactions, etc. (Fig. 5). Consequently, this method enables us to compare the output of FCS experiments with predictions obtained in a highly controlled environment with complex geometries where the molecule distribution, diffusion, photochemical properties and interspecies reactions can be precisely defined.

## 3. Materials and methods

### 3.1. Image acquisition and single-point FCS settings

A FV1000 laser scanning microscope (Olympus, Japan) equipped with an UPlanSApo 60× oil immersion objective (NA = 1.35) was set as follows for FCS assays:

- GFP and mCherry probes were excited using a multi-line Ar laser at 488 nm and a He-Ne green laser at 543 nm, respectively. The average power at the sample was 2 μW for both lasers.
- The 488/543 excitation dichroic mirror was used to direct the lasers to the sample and transmit the fluorescence.

- The pinhole size was set to 105 μm (~1 Airy unit).
- The fluorescence emitted by GFP and mCherry was split with a SDM560 dichroic mirror into two photomultiplier detectors set in the pseudo photon-counting detection mode and equipped with spectral filters tuned at 500–530 nm and 600–700 nm for GFP and mCherry channels, respectively.
- The microscope was set to collect a time trace at a fixed position ("point mode") selected by the user with a pixel dwell time of 20 μs.
- Finally, the total time of the experiment was set to acquire $8 \times 10^6$ data points (maximum number allowed in times series acquisition).

### 3.2. Sample preparation

#### 3.2.1. Plasmid constructs

pEGFP-GR was kindly provided by Mario Galigniana [104]. pmCherry-NCoA2 [105] and pmCherry-GR [56] were kind gifts from Gordon Hager. pH2B-mCherry, pEGFP-C3 and pmCherry-C1 were obtained from Addgene. The plasmids were purified from large E. coli cultures with a method that includes precipitation with polyethylene glycol and removal of RNA by precipitation with LiCl [106] with some modifications. High amounts of purified DNA stock solutions were obtained (1–5 mg; 260/280 nm absorbance ratio between 1.8 and 2).

#### 3.2.2. Cell culture, transfection and hormone treatment

Newborn Hamster Kidney (BHK) cells were cultured in Dulbecco's modified Eagle's medium (DMEM) (Thermo Fisher Scientific, Waltham, MA, USA) supplemented with 10% fetal bovine serum (FBS) (Internegocios, Mercedes, Argentina) plus penicillin (100 IU/ml) and streptomycin (100 μg/ml) at 37 °C under humidified atmosphere with 4.5% $CO_2$. The following protocol was used to prepare the cells for imaging:

- 0.13–0.17 mm thick cover glasses (round, 24 mm diameter) were sterilized by washing with ethanol and exposing to UV for 20 min on 6-well plates.
- 300,000 BHK cells per well were plated onto the coverslips, in DMEM supplemented with 10% FBS plus penicillin (100 IU/ml) and streptomycin (100 μg/ml).
- Cells were grown for 16–24 h before transfection.
- For each well, 1 μl of Lipofectamine 2000 (Thermo Fisher Scientific, Waltham, MA, USA) was diluted in 25 μl of DMEM and 1 μg of plasmid DNA was diluted in 25 μl of DMEM.
- The DNA solution was added dropwise to Lipofectamine solution and mixed gently.
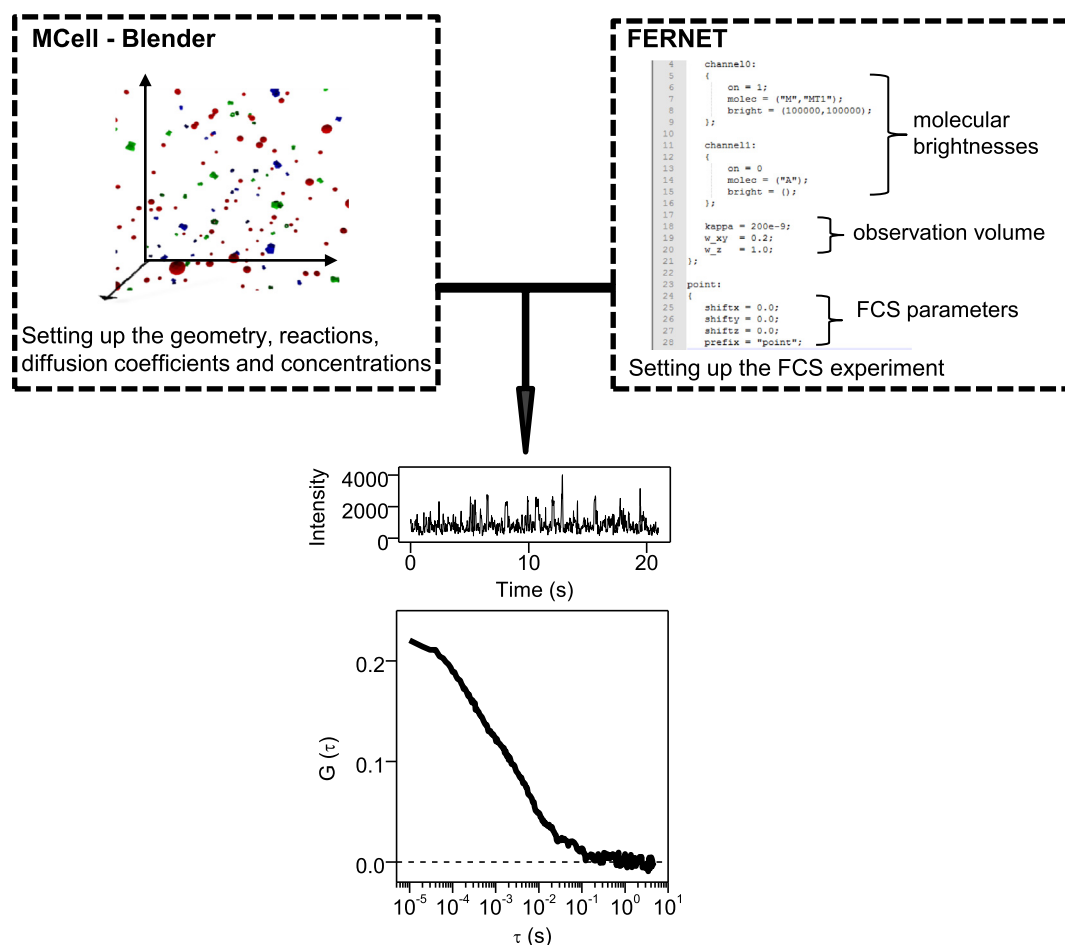- Growing medium was replaced by DMEM, without FBS or antibiotics.

**Fig. 5.** Representative example of the application of FERNET platform for FCS simulations. MCell-Cell Blender representation of molecules diffusing in 3D (red) and interacting with short-lived (green) and long-lived (blue) fixed targets randomly located in the box (left panel). Dark symbols illustrate occupied sites. The screenshot of the FERNET routine (right panel) shows the settings of the simulated FCS experiment. The fluorescence intensity time trace was obtained and analyzed with the SimFCS program to calculate the autocorrelation function (bottom panel). (For interpretation of the references to color in this figure legend, the reader is referred to the web version of this article.)

- After 20 min of incubation at room temperature, the DNA/Lipofectamine mix was added dropwise to the cells.
- After 6 h of incubation, the transfection medium was replaced by DMEM.
- Cells were incubated overnight. Then, dexamethasone (Sigma-Aldrich, St. Louis, MO, USA) was added in a concentration of 10 nM to cells transfected with GFP-GR. Cells were incubated at least 30 min with the hormone at 37 °C before imaging.

After incubation, the coverslips were placed in a home-made round aluminum chamber adapted to fit into the microscope stage and covered with culture medium. Cells presenting relative low fluorescence intensity (3 < signal/background < 30) were selected for FCS experiments.

### 3.3. Data analysis

- The data files were opened into the two channels in the "Huge vector" window of SimFCS. There, the intensity traces were visualized and checked for photobleaching, cell motion or any perturbation that could affect clearly the intensity trace (see Section 2.3).
- The individual ACFs (one for each channel) and the cross-correlation function were calculated with the "Large vector correlation" tool. There, the sampling frequency (50,000 s$^{-1}$) and the segment length (512,000 data points) in which the intensity

trace is divided were selected. This gives 15 segments to calculate CFs and average. In this instance, also some segments can be discarded if the user detects photobleaching or an outlier (see Section 2.3).
- Then, the average correlation functions were saved as text files. For the interpretation of ACF data, this data was analyzed using an extended version of the reaction dominant model described in [28] that considers binding to two populations of fixed sites (Table 2).

For each condition, the ACFs were fitted with this equation applying a global routine in MATLAB assuming a common residence time (fast and slow) for every single measurement in the same condition.

The interaction between GFP- and mCherry-fused proteins was quantified by the determination of an apparent association constant $K_{app}$ (see Section 2.2.4.2), assuming a 1:1 stoichiometry.

### 3.4. Simulation of FCS measurements with MCell-FERNET

For these particular simulations, we considered a simple system with two populations of static binding sites with different affinities for a single population of molecules.

To simplify the interpretation of the simulated data, we normally set the initial concentrations of all the species to those

obtained in the equilibrium. Thus, we pre-run MCell and analyze the time trace of the species until reaching the equilibrium conditions as described below. These values are then input in the MCell-FERNET platform.

- A box with 3.0 μm side was set as the reaction volume in the Scene_geometry file.
- A time step of $1 \times 10^{-5}$ s and $5 \times 10^6$ iterations were selected in the Scene_main file.
- 188 free molecules, 40 molecules bound to fast sites, 40 molecules bound to slow sites, 1585 free fast binding sites and 1858 free slow binding sites were released with the Scene_main file.
- A diffusion coefficient of $4 \times 10^{-7}$ cm²/s for free molecules was set in the Scene_molecules file. The diffusion coefficient for other species was set to zero.
- The reversible association reactions of the free molecules to the fast and the slow binding sites were defined in the Scene_reactions file with $k_{on}$ and $k_{off}$ values of $10^8$ M⁻¹ s⁻¹ and 50 s⁻¹ or $10^7$ M⁻¹ s⁻¹ and 5 s⁻¹, respectively.
- The time evolution of the concentrations of every species was followed with the Scene.rxn_output file. This MCell simulation can be run to check that these are equilibrium conditions. Then, FERNET simulation was run to simulate fluorescence acquisition:
- Free and bound molecules were selected as emitting fluorescence in one channel, with a brightness of $10^5$ cpms.
- Radial and axial waists of the PSF were set to 0.2 and 1.0 μm, respectively.
- 25 single-point measurements separated in 0.2 μm were recorded simultaneously in the "multi point" mode of FERNET.

This simulation was repeated 3–5 times with different initial seeds for statistical purpose.

## 4. Conclusions and perspectives

The complexity of nuclear organization is a fascinating subject that sheds light in a number of biochemical processes and its relevance in the regulation of nuclear processes. Advanced microscopy techniques are helping researchers in this long journey and reveal exciting aspects on the dynamics of nuclear processes such as transcription, replication and DNA repair.

Fluorescence fluctuations based methods have shown to be relevant tools for the study of many aspects of the nucleus ranging from the exploration of the rheological properties of the intranuclear milieu [11,13] to the interactions of proteins with chromatin [23]. From these studies, it became clearer that processes in the cell nucleus do not follow the simple mechanisms derived from bulk and cell-free assays. In the particular case of transcription, FCS techniques are helping us to understand how TFs dynamically interact with the complex chromatin landscape. It is now becoming accepted that TFs partition among different nuclear compartments and chromatin-binding sites with different relative affinities ultimately regulates their interactions with more specific sites [107]. Moreover, cofactors and other molecules relevant to transcription may interact with the TFs and modify their relative distribution among the nuclear compartments [23] affecting the final transcription output. However, conclusions reached in cell culture models should not be directly extrapolate to the physiological condition. Indeed, chromatin-protein interactions depend on the cell type, the cellular state and the properties of the extracellular milieu. Thus, the parameters describing the dynamics of protein-DNA interactions derived from FCS measurements (i.e.

bound fractions, residence times) should not be considered universal instead they are specific of the studied cell system.

The simplicity of FCS data acquisition, the high temporal resolution and wide time window attainable with these methodologies determined that FCS approaches are very popular in the field. We should emphasize that most FCS analyses rely on modeling the process(es) hidden in the intensity fluctuations thus, control or complementary experiments are frequently required to validate the theoretical model. In addition, the autocorrelation analysis implies averaging the behavior of population of molecules in a diffraction-limited region of the sample and therefore it is not possible distinguishing heterogeneities within this small volume.

In this article, we have focused the description on single-point FCS analyses in a commercial confocal microscope, however other fluctuation-based techniques such as scanning FCS [23], raster image correlation spectroscopy (RICS, [108]), mean square displacement from imaging (iMSD, [109]) and number and brightness method (N&B, [56]) can be instrumented in this simple setups making them accessible to the non-specialized scientific community.

Moreover, the combination of these fluctuation-based techniques with light sheet microscopy approaches are rapidly evolving and open the possibility to map the nuclear space dynamics pixel-by-pixel (e.g. [110]). We believe that these exciting new tools will contribute to achieve the ultimate goal of understanding the complex network of interactions of biomolecules in the cell nucleus and to generate detailed models of nuclear function.

## References

[1] A.D. Schmitt, M. Hu, B. Ren, Genome-wide mapping and analysis of chromosome architecture, Nat. Rev. Mol. Cell Biol. 17 (12) (2016) 743–755.

[2] D.M. Presman, D.A. Ball, V. Paakinaho, J.B. Grimm, L.D. Lavis, T.S. Karpova, G.L. Hager, Quantifying transcription factor binding dynamics at the single-molecule level in live cells, Methods 123 (2017) 76–88.

[3] C. Lanctot, T. Cheutin, M. Cremer, G. Cavalli, T. Cremer, Dynamic genome architecture in the nuclear space: regulation of gene expression in three dimensions, Nature reviews, Genetics 8 (2) (2007) 104–115.

[4] D. Zink, T. Cremer, Cell nucleus: chromosome dynamics in nuclei of living cells, Curr. Biol. 8 (9) (1998) R321–R324.

[5] H.A. Foster, J.M. Bridger, The genome and the nucleus: a marriage made by evolution. Genome organisation and nuclear architecture, Chromosoma 114 (4) (2005) 212–229.

[6] J.M. Zullo, I.A. Demarco, R. Pique-Regi, D.J. Gaffney, C.B. Epstein, C.J. Spooner, T.R. Luperchio, B.E. Bernstein, J.K. Pritchard, K.L. Reddy, H. Singh, DNA sequence-dependent compartmentalization and silencing of chromatin at the nuclear lamina, Cell 149 (7) (2012) 1474–1487.

[7] C. Randise-Hinchliff, J.H. Brickner, Transcription factors dynamically control the spatial organization of the yeast genome, Nucleus 7 (4) (2016) 369–374.

[8] S.M. Gasser, Visualizing chromatin dynamics in interphase nuclei, Science 296 (5572) (2002) 1412–1416.

[9] Y. Tseng, J.S. Lee, T.P. Kole, I. Jiang, D. Wirtz, Micro-organization and visco-elasticity of the interphase nucleus revealed by particle nanotracking, J. Cell Sci. 117 (Pt 10) (2004) 2159–2167.

[10] M. Baum, F. Erdel, M. Wachsmuth, K. Rippe, Retrieving the intracellular topology from multi-scale protein mobility mapping in living cells, Nat. Commun. 5 (2014) 4494.

[11] A. Bancaud, S. Huet, N. Daigle, J. Mozziconacci, J. Beaudouin, J. Ellenberg, Molecular crowding affects diffusion and binding of nuclear proteins in heterochromatin and reveals the fractal organization of chromatin, Embo J. 28 (24) (2009) 3785–3798.

[12] E. Hinde, F. Cardarelli, M.A. Digman, E. Gratton, In vivo pair correlation analysis of EGFP intranuclear diffusion reveals DNA-dependent molecular flow, Proc. Natl. Acad. Sci. U.S.A. 107 (38) (2010) 16560–16565.

[13] C. Di Rienzo, V. Piazza, E. Gratton, F. Beltram, F. Cardarelli, Probing short-range protein Brownian motion in the cytoplasm of living cells, Nat. Commun. 5 (2014) 5891.

[14] Y.S. Mao, B. Zhang, D.L. Spector, Biogenesis and function of nuclear bodies, Trends Genet. 27 (8) (2011) 295–306.

[15] J.C. Politz, R.A. Tuft, K.V. Prasanth, N. Baudendistel, K.E. Fogarty, L.M. Lifshitz, J. Langowski, D.L. Spector, T. Pederson, Rapid, diffusional shuttling of poly(A) RNA between nuclear speckles and the nucleoplasm, Mol. Biol. Cell 17 (3) (2006) 1239–1249.

[16] J.E. Sleeman, L. Trinkle-Mulcahy, Nuclear bodies: new insights into assembly/dynamics and disease relevance, Curr. Opin. Cell Biol. 28 (Supplement C) (2014) 76–83.

[17] D. Stanek, A.H. Fox, Nuclear bodies: news insights into structure and function, Curr. Opin. Cell Biol. 46 (2017) 94–101.

[18] Melanie D. White, Juan F. Angiolini, Yanina D. Alvarez, G. Kaur Ziqing, W. Zhao, E. Mocskos, L. Bruno, S. Bissiere, V. Levi, N. Plachta, Long-lived binding of Sox2 to DNA predicts cell fate in the four-cell mouse embryo, Cell 165 (1) (2016) 75–87.

[19] S.R. Yu, M. Burkhardt, M. Nowak, J. Ries, Z. Petrasek, S. Scholpp, P. Schwille, M. Brand, Fgf8 morphogen gradient forms by a source-sink mechanism with freely diffusing molecules, Nature 461 (7263) (2009) 533–536.

[20] A. Papantonis, P.R. Cook, Transcription factories: genome organization and gene regulation, Chem. Rev. 113 (11) (2013) 8683–8705.

[21] T. Misteli, Beyond the sequence: cellular organization of genome function, Cell 128 (4) (2007) 787–800.

[22] B. van Steensel, M. Brink, K. van der Meulen, E.P. van Binnendijk, D.G. Wansink, L. de Jong, E.R. de Kloet, R. van Driel, Localization of the glucocorticoid receptor in discrete clusters in the cell nucleus, J. Cell Sci. 108 (Pt 9) (1995) 3003–3011.

[23] M. Stortz, D.M. Presman, L. Bruno, P. Annibale, M.V. Dansey, G. Burton, E. Gratton, A. Pecci, V. Levi, Mapping the dynamics of the glucocorticoid receptor within the nuclear landscape, Sci. Rep. 7 (1) (2017) 6219.

[24] F. Mueller, D. Mazza, T.J. Stasevich, J.G. McNally, FRAP and kinetic modeling in the analysis of nuclear protein dynamics: what do we really know?, Curr Opin. Cell Biol. 22 (3) (2010) 403–411.

[25] L. Schmiedeberg, K. Weisshart, S. Diekmann, G. Meyer Zu Hoerste, P. Hemmerich, High- and low-mobility populations of HP1 in heterochromatin of mammalian cells, Mol. Biol. Cell 15 (6) (2004) 2819–2833.

[26] S. Mikuni, M. Tamura, M. Kinjo, Analysis of intranuclear binding process of glucocorticoid receptor using fluorescence correlation spectroscopy, FEBS Lett. 581 (3) (2007) 389–393.

[27] D. Mazza, T.J. Stasevich, T.S. Karpova, J.G. McNally, Monitoring dynamic binding of chromatin proteins in vivo by fluorescence correlation spectroscopy and temporal image correlation spectroscopy, Meth. Mol. Biol. 833 (2012) 177–200.

[28] A. Michelman-Ribeiro, D. Mazza, T. Rosales, T.J. Stasevich, H. Boukari, V. Rishi, C. Vinson, J.R. Knutson, J.G. McNally, Direct measurement of association and dissociation rates of DNA binding in live cells by fluorescence correlation spectroscopy, Biophys. J. 97 (1) (2009) 337–346.

[29] F.L. Groeneweg, M.E. van Royen, S. Fenz, V.I. Keizer, B. Geverts, J. Prins, E.R. de Kloet, A.B. Houtsmuller, T.S. Schmidt, M.J. Schaaf, Quantitation of glucocorticoid receptor DNA-binding dynamics by single-molecule microscopy and FRAP, PLoS One 9 (3) (2014) e90532.

[30] T. Morisaki, W.G. Muller, N. Golob, D. Mazza, J.G. McNally, Single-molecule analysis of transcription factor binding at transcription sites in live cells, Nat. Commun. 5 (2014) 4456.

[31] V. Paakinaho, D.M. Presman, D.A. Ball, T.A. Johnson, R.L. Schiltz, P. Levitt, D. Mazza, T. Morisaki, T.S. Karpova, G.L. Hager, Single-molecule analysis of steroid receptor and cofactor action in living cells, Nat. Commun. 8 (2017) 15896.

[32] A.B. Houtsmuller, Fluorescence recovery after photobleaching: application to nuclear proteins, Adv. Biochem. Eng. Biotechnol. 95 (2005) 177–199.

[33] M.A. Digman, E. Gratton, Lessons in fluctuation correlation spectroscopy, Annu. Rev. Phys. Chem. 62 (2011) 645–668.

[34] V. Levi, E. Gratton, Exploring dynamics in living cells by tracking single particles, Cell. Biochem. Biophys. 48 (1) (2007) 1–15.

[35] M.A. Digman, E. Gratton, Imaging barriers to diffusion by pair correlation functions, Biophys. J. 97 (2) (2009) 665–673.

[36] B. Hebert, S. Costantino, P.W. Wiseman, Spatiotemporal image correlation spectroscopy (STICS) theory, verification, and application to protein velocity mapping in living CHO cells, Biophys. J. 88 (5) (2005) 3601–3614.

[37] P.N. Hedde, M. Stakic, E. Gratton, Rapid measurement of molecular transport and interaction inside living cells using single plane illumination, Sci. Rep. 4 (2014) 7048.

[38] P.W. Wiseman, Image correlation spectroscopy: mapping correlations in space, time, and reciprocal space, Meth. Enzymol. 518 (2013) 245–267.

[39] E.L. Elson, Fluorescence correlation spectroscopy: past, present, future, Biophys. J. 101 (12) (2011) 2855–2870.

[40] J. Enderlein, I. Gregor, D. Patra, J. Fitter, Art and artefacts of fluorescence correlation spectroscopy, Curr. Pharm. Biotechnol. 5 (2) (2004) 155–161.

[41] J. Speil, E. Baumgart, J.P. Siebrasse, R. Veith, U. Vinkemeier, U. Kubitscheck, Activated STAT1 transcription factors conduct distinct saltatory movements in the cell nucleus, Biophys. J. 101 (11) (2011) 2592–2600.

[42] J.B. Grimm, B.P. English, J. Chen, J.P. Slaughter, Z. Zhang, A. Revyakin, R. Patel, J.J. Macklin, D. Normanno, R.H. Singer, T. Lionnet, L.D. Lavis, A general method to improve fluorophores for live-cell and single-molecule microscopy, Nat. Meth. 12 (3) (2015) 244–250. 3 p following 250.

[43] R.Y. Tsien, The green fluorescent protein, Annu. Rev. Biochem. 67 (1998) 509–544.

[44] J. Zhang, R.E. Campbell, A.Y. Ting, R.Y. Tsien, Creating new fluorescent probes for cell biology, Nat. Rev. Mol. Cell Biol. 3 (12) (2002) 906–918.

[45] J. Lippincott-Schwartz, G.H. Patterson, Development and use of fluorescent protein markers in living cells, Science 300 (5616) (2003) 87–91.

[46] K.M. Dean, A.E. Palmer, Advances in fluorescence labeling strategies for dynamic cellular imaging, Nat. Chem. Biol. 10 (7) (2014) 512–523.

[47] A. Diaspro, G. Chirico, M. Collini, Two-photon fluorescence excitation and related techniques in biological microscopy, Q. Rev. Biophys. 38 (2) (2005) 97–166.

[48] V. Anderson, Principal factors influencing the accuracy of FCS data, in: D.R.f.B. I.O.-E.D.C. University (Ed.).

[49] E.M. Smith, J.D. Mueller, The statistics of protein expression ratios for cellular fluorescence studies, Eur. Biophys. J. 41 (3) (2012) 341–352.

[50] R.M. Mortensen, R.E. Kingston, Selection of transfected mammalian cells, Curr. Protoc. Mol. Biol. Chapter 9, 2009. Unit9 5.

[51] J.D. Sander, J.K. Joung, CRISPR-Cas systems for editing, regulating and targeting genomes, Nat. Biotechnol. 32 (4) (2014) 347–355.

[52] P.D. Hsu, E.S. Lander, F. Zhang, Development and applications of CRISPR-Cas9 for genome engineering, Cell 157 (6) (2014) 1262–1278.

[53] M. Ratz, I. Testa, S.W. Hell, S. Jakobs, CRISPR/Cas9-mediated endogenous protein tagging for RESOLFT super-resolution microscopy of living human cells, Sci. Rep. 5 (2015) 9592.

[54] B. Chen, L.A. Gilbert, B.A. Cimini, J. Schnitzbauer, W. Zhang, G.W. Li, J. Park, E. H. Blackburn, J.S. Weissman, L.S. Qi, B. Huang, Dynamic imaging of genomic loci in living human cells by an optimized CRISPR/Cas system, Cell 155 (7) (2013) 1479–1491.

[55] E. Snapp, Design and use of fluorescent fusion proteins in cell biology, Curr. Protoc. Cell Biol. Chapter 21, 2005. Unit 21 4.

[56] D.M. Presman, M.F. Ogara, M. Stortz, L.D. Alvarez, J.R. Pooley, R.L. Schiltz, L. Grontved, T.A. Johnson, P.R. Mittelstadt, J.D. Ashwell, S. Ganesan, G. Burton, V. Levi, G.L. Hager, A. Pecci, Live cell imaging unveils multiple domain requirements for in vivo dimerization of the glucocorticoid receptor, PLoS Biol. 12 (3) (2014) e1001813.

[57] H. Htun, J. Barsony, I. Renyi, D.L. Gould, G.L. Hager, Visualization of glucocorticoid receptor translocation and intranuclear organization in living cells with a green fluorescent protein chimera, Proc. Natl. Acad. Sci. U.S.A. 93 (10) (1996) 4845–4850.

[58] J. Wiedenmann, F. Oswald, G.U. Nienhaus, Fluorescent proteins for live cell imaging: opportunities, limitations, and challenges, IUBMB Life 61 (11) (2009) 1029–1042.

[59] T.J. Gibson, M. Seiler, R.A. Veitia, The transience of transient overexpression, Nat. Meth. 10 (8) (2013) 715–721.

[60] C.A. Lo, I. Kays, F. Emran, T.J. Lin, V. Cvetkovska, B.E. Chen, Quantification of protein levels in single living cells, Cell Rep. 13 (11) (2015) 2634–2644.

[61] Y. Chen, J.D. Muller, P.T. So, E. Gratton, The photon counting histogram in fluorescence fluctuation spectroscopy, Biophys. J. 77 (1) (1999) 553–567.

[62] M.A. Digman, R. Dalal, A.F. Horwitz, E. Gratton, Mapping the number of molecules and brightness in the laser scanning microscope, Biophys. J. 94 (6) (2008) 2320–2332.

[63] V.C. Coffman, J.Q. Wu, Counting protein molecules using quantitative fluorescence microscopy, Trends Biochem. Sci. 37 (11) (2012) 499–506.

[64] A. Furtado, R. Henry, Measurement of green fluorescent protein concentration in single cells by image analysis, Anal. Biochem. 310 (1) (2002) 84–92.

[65] A.H. Fischer, K.A. Jacobson, J. Rose, R. Zeller, Preparation of slides and coverslips for microscopy, CSH Protoc. (2008) (2008) pdb prot4988.

[66] K.M. Berland, P.T. So, E. Gratton, Two-photon fluorescence correlation spectroscopy: method and application to the intracellular environment, Biophys. J. 68 (2) (1995) 694–701.

[67] R. Rigler, U. Mets, J. Widengren, P. Kask, Fluorescence correlation spectroscopy with high count rate and low background: analysis of translational diffusion, Eur. Biophys. J. 22 (1993) 169–175.

[68] E.L. Elson, Brief introduction to fluorescence correlation spectroscopy, Meth. Enzymol. 518 (2013) 11–41.

[69] S.M. Guo, N. Bag, A. Mishra, T. Wohland, M. Bathe, Bayesian total internal reflection fluorescence correlation spectroscopy reveals hIAPP-induced plasma membrane domain organization in live cells, Biophys. J. 106 (1) (2014) 190–200.

[70] S.M. Guo, J. He, N. Monnier, G. Sun, T. Wohland, M. Bathe, Bayesian approach to the analysis of fluorescence correlation spectroscopy data II: application to simulated and in vitro data, Anal. Chem. 84 (9) (2012) 3880–3888.

[71] T. Wohland, X. Shi, J. Sankaran, E.H. Stelzer, Single plane illumination fluorescence correlation spectroscopy (SPIM-FCS) probes inhomogeneous three-dimensional environments, Opt. Express 18 (10) (2010) 10627–10641.

[72] L. Kastrup, H. Blom, C. Eggeling, S.W. Hell, Fluorescence fluctuation spectroscopy in subdiffraction focal volumes, Phys. Rev. Lett. 94 (17) (2005) 178104.

[73] M.J. Levene, J. Korlach, S.W. Turner, M. Foquet, H.G. Craighead, W.W. Webb, Zero-mode waveguides for single-molecule analysis at high concentrations, Science 299 (5607) (2003) 682–686.

[74] S.T. Hess, W.W. Webb, Focal volume optics and experimental artifacts in confocal fluorescence correlation spectroscopy, Biophys. J. 83 (4) (2002) 2300–2317.

[75] M.J. Booth, T. Wilson, Refractive-index-mismatch induced aberrations in single-photon and two-photon microscopy and the use of aberration correction, J. Biomed. Opt. 6 (3) (2001) 266–272.

[76] E.M. Manders, A.E. Visser, A. Koppen, W.C. de Leeuw, R. van Liere, G.J. Brakenhoff, R. van Driel, Four-dimensional imaging of chromatin dynamics during the assembly of the interphase nucleus, Chromosome Res. 11 (5) (2003) 537–547.

[77] J.B. Sibarita, Deconvolution microscopy, Adv. Biochem. Eng. Biotechnol. 95 (2005) 201–243.

[78] R.W. Cole, T. Jinadasa, C.M. Brown, Measuring and interpreting point spread functions to determine confocal microscope resolution and ensure quality control, Nat. Protoc. 6 (12) (2011) 1929–1941.

[79] S.A. Kim, K.G. Heinze, P. Schwille, Fluorescence correlation spectroscopy in living cells, Nat. Meth. 4 (11) (2007) 963–973.

[80] P. Kapusta, Absolute Diffusion Coefficients: Compilation of Reference Data for FCS Calibration, PicoQuant GmbH, 2010.

[81] T. Maeda, M.J. Lee, G. Palczewska, S. Marsili, P.J. Tesar, K. Palczewski, M. Takahashi, A. Maeda, Retinal pigmented epithelial cells obtained from human induced pluripotent stem cells possess functional visual cycle enzymes in vitro and in vivo, J. Biol. Chem. 288 (48) (2013) 34484–34493.

[82] I. Axelsson, Characterization of proteins and other macromolecules by agarose gel chromatography, J. Chromatogr. 152 (1978) 21–32.

[83] A. Einstein, Investigations on the theory of the brownian movement, Dover Edition., 1956.

[84] U. Anand, C. Jash, S. Mukherjee, Protein unfolding and subsequent refolding: a spectroscopic investigation, Phys. Chem. Chem. Phys. 13 (45) (2011) 20418–20426.

[85] J. Enderlein, I. Gregor, Using fluorescence lifetime for discriminatinng detector afterpulsing in fluorescence correlation spectroscopy, Rev. Sci. Instrum 76 (2005) 033102.

[86] M. Zhao, L. Jin, B. Chen, Y. Ding, H. Ma, D. Chen, Afterpulsing and its correction in fluorescence correlation spectroscopy experiments, Appl. Opt. 42 (19) (2003) 4031–4036.

[87] A. Tcherniak, C. Reznik, S. Link, C.F. Landes, Fluorescence correlation spectroscopy: criteria for analysis in complex systems, Anal. Chem. 81 (2) (2009) 746–754.

[88] S. Matsuo, H. Misawa, Direct measurement of laser power through a high numerical aperture oil immersion objective lens using a solid immersion lens, Rev. Sci. Instrum. 73 (5) (2002).

[89] K. Bacia, S.A. Kim, P. Schwille, Fluorescence cross-correlation spectroscopy in living cells, Nat. Meth. 3 (2) (2006) 83–89.

[90] P. Schwille, E. Haustein, Fluorescence Correlation Spectroscopy: An Introduction to its Concepts and Applications Biophys Textbook Online, 2001.

[91] J.R. Lakowicz, Principles of Fluorescence Spectroscopy, 3rd ed., Springer, 2006.

[92] M. Tiwari, S. Mikuni, H. Muto, M. Kinjo, Determination of dissociation constant of the NFkappaB p50/p65 heterodimer using fluorescence cross-correlation spectroscopy in the living cell, Biochem. Biophys. Res. Commun. 436 (3) (2013) 430–435.

[93] K. Bacia, P. Schwille, Practical guidelines for dual-color fluorescence cross-correlation spectroscopy, Nat. Protoc. 2 (11) (2007) 2842–2856.

[94] P. Muller, P. Schwille, T. Weidemann, PyCorrFit-generic data evaluation for fluorescence correlation spectroscopy, Bioinformatics 30 (17) (2014) 2532–2533.

[95] M.A. Digman, C.M. Brown, A.R. Horwitz, W.W. Mantulin, E. Gratton, Paxillin dynamics measured during adhesion assembly and disassembly by correlation spectroscopy, Biophys. J. 94 (7) (2008) 2819–2831.

[96] N.L. Thompson, Fluorescence correlation spectroscopy, in: J.R. Lakowicz (Ed.), Topics in Fluorescence Spectroscopy, Plenum Press, New York, 1991, pp. 337–378.

[97] M.J. Saxton, Anomalous diffusion due to binding: a Monte Carlo study, Biophys. J. 70 (3) (1996) 1250–1262.

[98] M.J. Saxton, Anomalous diffusion due to obstacles: a Monte Carlo study, Biophys. J. 66 (2 Pt 1) (1994) 394–401.

[99] K.G. Konishi S, Information Criteria and Statistical Modeling, Springer, 2008.

[100] J.F. Angiolini, N. Plachta, E. Mocskos, V. Levi, Exploring the dynamics of cell processes through simulations of fluorescence microscopy experiments, Biophys. J. 108 (2015) 2613–2618.

[101] R.A. Kerr, T.M. Bartol, B. Kaminsky, M. Dittrich, J.C. Chang, S.B. Baden, T.J. Sejnowski, J.R. Stiles, Fast Monte Carlo simulation methods for biological reaction-diffusion systems in solution and on surfaces, SIAM J. Sci. Comput. 30 (6) (2008) 3126.

[102] J.R. Stiles, T.M. Bartol, Monte Carlo methods for simulating realistic synaptic microphysiology using MCell, in: E. De Schutter (Ed.), Computational Neuroscience: Realistic Modeling for Experimentalists, CRC Press, Boca Raton, 2001, pp. 87–127.

[103] J.R. Stiles, D. Van Helden, T.M. Bartol Jr., E.E. Salpeter, M.M. Salpeter, Miniature endplate current rise times less than 100 microseconds from improved dual recordings can be modeled with passive acetylcholine diffusion from a synaptic vesicle, Proc. Natl. Acad. Sci. U.S.A. 93 (12) (1996) 5747–5752.

[104] M.D. Galigniana, J.L. Scruggs, J. Herrington, M.J. Welsh, C. Carter-Su, P.R. Housley, W.B. Pratt, Heat shock protein 90-dependent (geldanamycin-inhibited) movement of the glucocorticoid receptor through the cytoplasm to the nucleus requires intact cytoskeleton, Mol. Endocrinol. 12 (12) (1998) 1903–1913.

[105] T.C. Voss, R.L. Schiltz, M.H. Sung, T.A. Johnson, S. John, G.L. Hager, Combinatorial probabilistic chromatin interactions produce transcriptional heterogeneity, J. Cell Sci. 122 (Pt 3) (2009) 345–356.

[106] D. Pulleyblank, M. Michalak, S.L. Daisley, R. Glick, A method for the purification of E. coli plasmid DNA by homogeneous lysis and polyethylene glycol precipitation, Mol. Biol. Rep. 9 (3) (1983) 191–195.

[107] F. Mueller, T.J. Stasevich, D. Mazza, J.G. McNally, Quantifying transcription factor kinetics: at work or at play?, Crit Rev. Biochem. Mol. Biol. 48 (5) (2013) 492–514.

[108] C.M. Brown, R.B. Dalal, B. Hebert, M.A. Digman, A.R. Horwitz, E. Gratton, Raster image correlation spectroscopy (RICS) for measuring fast protein dynamics and concentrations with a commercial laser scanning confocal microscope, J. Microsc. 229 (Pt 1) (2008) 78–91.

[109] C. Di Rienzo, E. Gratton, F. Beltram, F. Cardarelli, From fast fluorescence imaging to molecular diffusion law on live cell membranes in a commercial microscope, J. Vis. Exp. 92 (2014). e51994.

[110] A.P. Singh, R. Galland, M.L. Finch-Edmondson, G. Grenci, J.B. Sibarita, V. Studer, V. Viasnoff, T.E. Saunders, 3D protein dynamics in the cell nucleus, Biophys. J. 112 (1) (2017) 133–142.

[111] J.C. Gebhardt, D.M. Suter, R. Roy, Z.W. Zhao, A.R. Chapman, S. Basu, T. Maniatis, X.S. Xie, Single-molecule imaging of transcription factor binding to DNA in live mammalian cells, Nat. Meth. 10 (5) (2013) 421–426.

[112] V. Levi, Q. Ruan, M. Plutz, A.S. Belmont, E. Gratton, Chromatin dynamics in interphase cells revealed by tracking in a two-photon excitation microscope, Biophys. J. 89 (2005) 4275–4285.

[113] I. Izeddin, V. Recamier, L. Bosanac, I.I. Cisse, L. Boudarene, C. Dugast-Darzacq, F. Proux, O. Benichou, R. Voituriez, O. Bensaude, M. Dahan, X. Darzacq, Single-molecule tracking in live cells reveals distinct target-search strategies of transcription factors in the nucleus, Elife 3 (2014).

[114] Z.B. Katz, B.P. English, T. Lionnet, Y.J. Yoon, N. Monnier, B. Ovryn, M. Bathe, R.H. Singer, Mapping translation 'hot-spots' in live cells by tracking single molecules of mRNA and ribosomes, Elife 5 (2016).

[115] W.K. Cho, N. Jayanth, B.P. English, T. Inoue, J.O. Andrews, W. Conway, J.B. Grimm, J.H. Spille, L.D. Lavis, T. Lionnet, I.I. Cisse, RNA Polymerase II cluster dynamics predict mRNA output in living cells, Elife 5 (2016).

[116] R.D. Phair, T. Misteli, High mobility of proteins in the mammalian cell nucleus, Nature 404 (6778) (2000) 604–609.

[117] F. Mueller, P. Wach, J.G. McNally, Evidence for a common mode of transcription factor interaction with chromatin as revealed by improved quantitative fluorescence recovery after photobleaching, Biophys. J. 94 (8) (2008) 3323–3339.

[118] G. Kaur, M.W. Costa, C.M. Nefzger, J. Silva, J.C. Fierro-Gonzalez, J.M. Polo, T.D. Bell, N. Plachta, Probing transcription factor diffusion dynamics in the living mammalian embryo with photoactivatable fluorescence correlation spectroscopy, Nat. Commun. 4 (2013) 1637.